THE JOURNAL OF PHYSICAL CHEMISTRY A

ARTICLE

pubs.acs.org/JPCA

Environment-Dependent Ultrafast Photoisomerization Dynamics in Azo Dye

Chun-Chih Hsu,[†] Yu-Ting Wang,[†] Atsushi Yabushita,[*,†] Chih-Wei Luo,[*,†] Yi-Nan Hsiao,[†] Shiuan-Huei Lin,[†] and Takayoshi Kobayashi[†,‡,§]

[†]Department of Electrophysics, National Chiao-Tung University, Hsinchu, Taiwan, Republic of China

[‡]Department of Applied Physics and Chemistry and Institute for Laser Science, The University of Electro-Communications, Tokyo, Japan

[§]ICORP, JST, 4-1-8 Honcho, Kawaguchi, Saitama, 332-0012, Japan

ABSTRACT: Azoaromatic dyes have been extensively investigated over the past decade due to their potential use in a variety of optical devices that exploit their ultrafast photoisomerization processes. Among the azoaromatic dyes, Disperse Red 19 is a commercially available azobenzene nonlinear optical chromophore with a relatively high ground-state dipole moment. In the present study, we used ultrafast time-resolved spectroscopy to clarify the dynamics of a push−pull substituted azobenzene dye. Solution and film samples exhibited different ultrafast dynamics, indicating that the molecular environment affects the photoisomerization dynamics of the dye.

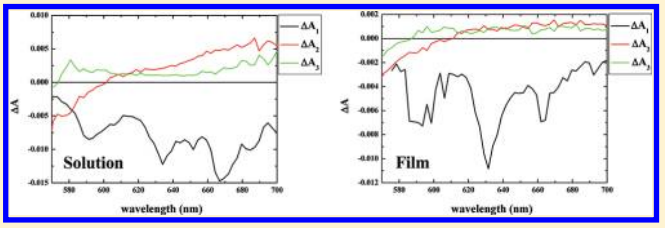

INTRODUCTION

Over the past decades, *trans*−*cis* photoisomerization has been one of the most widely investigated photochromic reactions. Azoaromatic dyes[1] are typical systems that exhibit *trans*−*cis* photoisomerization. They have been extensively investigated and various experimental techniques have been used to clarify the *trans*−*cis* photoisomerization mechanism.[2−4] Irradiation by linearly polarized light results in reversible *trans*−*cis*−*trans* isomerization via a hole-burning mechanism. This isomerization reorients the molecules, causing the dye to become birefringent by making the azobenzene groups sensitive to optical polarization.[5] Thus, azoaromatic dyes can be used in various applications such as dynamic volume holograms,[6,7] waveguide media,[8] and light-driven molecular scissors.[9] To improve their performance, it is essential to elucidate the ultrafast dynamics of the photoisomerization process. There have been several recent studies of the ultrafast dynamics of azobenzene dyes; for example, Koller et al.[10] used infrared spectroscopy to investigate 4-nitro-40-(dimethylamino)azobenzene and Poprawa-Smoluch et al.[11] used absorption spectroscopy to study Disperse Red 1. Disperse Red 19 (DR19) is a commercial azobenzene nonlinear optical chromophore with a large ground-state dipole moment of 8 D.[12,13] In the present report, we investigate the ultrafast dynamics of solution and film samples of DR19 using absorbance difference spectroscopy with a femtosecond time resolution.

EXPERIMENTAL SECTION

The azobenzene dye DR19 (dye content 95%) was purchased from Sigma-Aldrich Co. and used after recrystallization. A solution sample was prepared by dissolving 0.1 wt % DR19 in trimethylolpropane triglycidyl ether (TMTE; technical grade; Sigma-Aldrich). A polymer film sample of DR19 was prepared as follows: 0.1 wt % DR19 was dissolved in TMTE and a harden agent (1,2-diaminopropane). The solution was cast on a flat glass (doctor-Blade method)[14] to form a polymer film. The polymer film was estimated to have an average thickness of 0.5 mm by a slide caliper.

The solution and film samples were respectively stored in a sealed vial and a drybox in a dark-adaptive ambient until immediately prior to being used. Figure 1 shows stationary absorption spectrum of the solution and film samples. The absorption peaks at 494 and 500 nm for the solution and film samples, respectively, are due to the strongly allowed $\pi-\pi^*$ transition.[15]

Time-resolved spectroscopy of the samples was performed using ultrashort visible pulses generated by a noncollinear optical parametric amplifier[16,17] seeded by a 5 kHz regenerative Ti:sapphire amplifier (Coherent Inc. Legend-USP-HE). These ultrashort visible pulses had a broad spectrum that extended from 514 to 758 nm (see Figure 1). The instrument response time was adjusted to be 9 fs by monitoring the pulse width using second-harmonic-generation frequency-resolved optical gating (SHG-FROG) measurements[18] (see below).

In the pump−probe measurements of the solution sample, the pulse width was compressed to 9 fs in a 1-mm glass cell as follows. We first inserted a 1 mm thick glass plate in front of the entrance of the SHG-FROG system and adjusted pulse compressor to obtain 9 fs pulses. It set the pulse width to be 9 fs after passing through the 1 mm thick glass. The glass walls of the glass cell used

Received: June 1, 2011
Revised: September 14, 2011
Published: September 14, 2011

dx.doi.org/10.1021/jp2051307 | *J. Phys. Chem. A* 2011, 115, 11508–11514

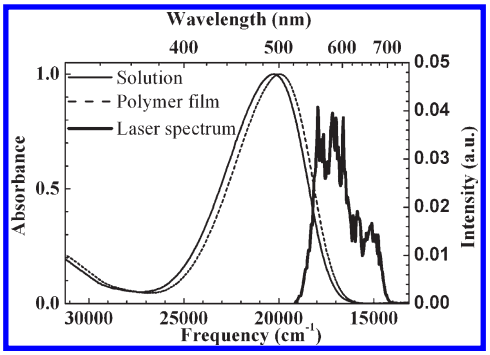

Figure 1. Normalized absorption spectra of DR19 in solution (solid line) and a polymer film (dashed line). The spectrum of NOPA output (thick solid line) used for both pump and probe pulses.

for the solution measurement have the same thickness of 1 mm. If the 1 mm thick glass is removed and the pulse comes into the glass cell, the pulse width becomes 9 fs inside the glass cell passing through one side of the 1 mm thick glass wall.

In the pump−probe measurements of the film sample, the pulse width was also adjusted to 9 fs without inserting any glass plate. Therefore, the instrument response time was 9 fs in both cases. The pump beam was focused to a 1.4×10^{-5} cm^2 spot. The pump and probe pulse energies were 8 and 0.8 nJ, respectively.

The probe pulse intensity at each probe wavelength was simultaneously detected by Si avalanche photodiodes attached to a monochromator (Princeton Instruments, SpectraPro 2300i). A mechanical chopper was inserted in the optical path of the pump pulse and was operated at a frequency of 2.5 kHz so that it was in synchronization with the laser pulses. Changes in the transmitted intensity of the probe pulse induced by the pump pulse were processed by a 96-channel lock-in amplifier referenced to the frequency and phase of the chopper. Preamplifiers were used to amplify the electric current measured by the avalanche photodiodes prior to lock-in detection. Because the preamplifier had a cutoff frequency of 5 kHz, harmonic noise of the 2.5 kHz reference frequency was not detected in the observed signals.

For time-resolved spectroscopy of the solution sample, the sample was placed in a 1 mm thick quartz flow cell (Starna Cells Inc., 48-Q-1; flow rate: 50 mL/min) and was recirculated by a peristaltic pump to ensure that each laser pulse irradiated a fresh sample. To prevent the photogenerated *cis*-isomer accumulating during measurements, the peristaltic pump was connected to a reservoir containing a large volume (60 mL) of the solution sample. During time-resolved measurements of the absorbance difference of the polymer film sample, the position of the sample was changed after each scan to ensure that photodamage did not accumulate during the measurement. Each scan of the time-resolved absorption difference spectra was performed in 5 s using a multiplex fast-scan system.[19] In the data analysis, we used data averaged over 40 scans. When the sample was irradiated at the same position for half an hour, the sample was damaged and caused strong scattering light. Meanwhile, the photodamage was negligible in the scan time of 5 s.

In the present measurement, the beam diameter on the sample is about 20 μm, which is about 10× larger than the period of the optically inscribed grating reported by Barrett et al.[20] Therefore, the sample still exists inside the beam spot even after the irradiation.

All experiments were performed at room temperature.

RESULTS AND DISCUSSION

Ultrafast Dynamics of the Solution Sample. Figure 2a shows a two-dimensional plot of absorbance difference (ΔA) spectrum of the DR19 solution sample measured for delays from −0.1 to 1.4 ps (short delay region) and probe wavelength from 514 to 758 nm. Figure 2b shows the ΔA spectrum measured between −1 and 14 ps (long delay region) in the same probe wavelength region. The black curves in Figure 2a,b are contours for which ΔA is zero. Figure 2c,d show ΔA traces for five different probe wavelengths in Figure 2a,b.

ΔA is generally negative at a probe wavelength below 580 nm. At these wavelengths, the ground state has an absorption band. Thus, ΔA is thought to be negative due to absorption bleaching, which implies that the electron population is depleted when DR19 is photoexcited by pump pulses. The positive ΔA observed at probe wavelengths longer than 580 nm was attributed to induced absorption of the excited state.

At first, we analyzed the exponential decays of the time traces to study the ultrafast dynamics of the electronic states during and after photoexcitation of DR19.

The ΔA traces in Figure 2c,d contain three decay components with lifetimes of ∼0.1, ∼1, and ∼10 ps. Therefore, the ΔA traces should be fitted by a triple exponential function given by

$$f(t,\lambda) = \Delta A_1(\lambda)e^{-t/\tau_1} + \Delta A_2(\lambda)e^{-t/\tau_2} + \Delta A_0(\lambda)e^{-t/\tau_3} \quad (\tau_1 < \tau_2 < \tau_3) \tag{1}$$

The τ_1 (∼0.1 ps) lifetime component decays, becoming negligible at delay longer than 0.4 ps. Therefore, we determined the other two time constants (τ_2 and τ_3) by fitting the ΔA trace in the long delay region between 0.4 and 14 ps using the following double exponential function

$$f(t,\lambda) = \Delta A_2(\lambda)e^{-t/\tau_2} + \Delta A_3(\lambda)e^{-t/\tau_3} \quad (\tau_2 < \tau_3) \tag{2}$$

Global fitting analysis estimated the time constants τ_2 and τ_3 to be 1.11 ± 0.13 and 4.65 ± 0.56 ps, respectively. Using the ΔA traces and the estimated time constants, the spectra of these lifetime components were calculated by the least-squares method (see Figure 3).

The instrument response time of the present measurements was estimated to be 9 fs, which is considered negligible for delays longer than 50 fs. Therefore, we determined the shortest time constant (τ_1) and its spectral component (ΔA_1) by fitting the ΔA trace in the short delay region from 50 fs to 1.4 ps. In the fitting analysis, we applied the global fitting using the following double exponential function by fixing the parameter τ_2 to 1.11 ps (as estimated above). Note that the τ_3 decay component can be considered constant for delays up to 1.4 ps. The function $f(t,\lambda)$ is given by

$$f(t,\lambda) = \Delta A_1(\lambda)e^{-t/\tau_1} + \Delta A_2(\lambda)e^{-t/\tau_2} + \Delta A_0(\lambda) \quad (\tau_1 < \tau_2) \tag{3}$$

where $\Delta A_0(\lambda)$ indicates a spectral component with an infinite lifetime. Global fitting analysis estimated the time constant τ_1 to be 104 ± 12 fs and its spectral component $\Delta A_1(\lambda)$ was obtained by the least-squares method (see Figure 3).

The shortest time constant, τ_1, had been only roughly estimated in previous studies because of their limited time resolutions. In the present study using a 9 fs pulse, τ_1 was accurately estimated to be 104 ± 12 fs. Its spectral component, $\Delta A_1(\lambda)$,

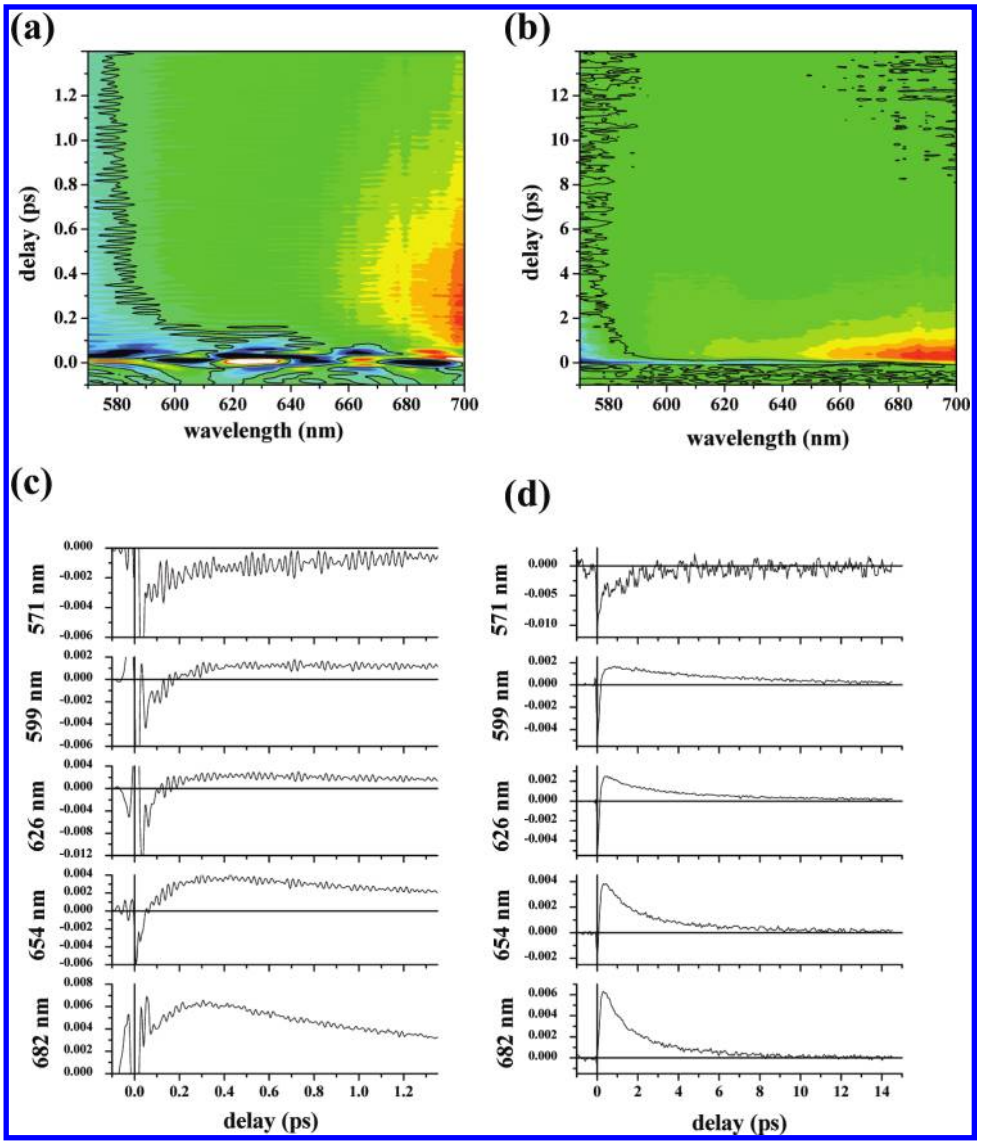

Figure 2. Measured 2D time-resolved absorbance difference spectra of DR19 in a solution sample (a) scanned from −0.1 to 1.4 ps and (b) that scanned from −1 to 14 ps. Black curves represent contours where the absorbance difference is zero ($\Delta A = 0$). (c, d) Time-resolved ΔA traces at five different probe wavelengths picked up from (a) and (b), respectively.

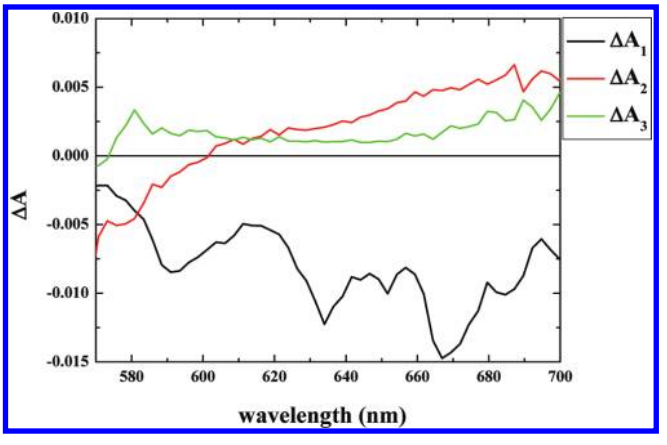

Figure 3. ΔA_1, ΔA_2, and ΔA_3 are spectral components of the DR19 solution sample, which decay with the lifetimes of τ_1, τ_2, and τ_2, respectively.

does not reflect the spectral profile of the stationary absorption spectrum shown in Figure 1. Therefore, the shortest decay component does not include decay to the electronic ground state and it was attributed to large amplitude wave packet motion on the excited-state potential surface out of the Franck−Condon (FC) region.[21] The negative spectrum of ΔA_1 is considered to be the stimulated emission spectrum of the FC state.

The time constant τ_2 was estimated to be 1.11 ± 0.13 ps. Its spectral component, $\Delta A_2(\lambda)$, is negative, reflecting the spectral profile of the stationary absorption spectrum at probe wavelengths shorter than 580 nm. Therefore, the wave packet generated by the photoexcitation is considered to be spread over the potential energy surface of the electronic excited state and to locate the conical intersection to the ground state via photoisomerization around the NN double bond; this process is responsible for the time constant of τ_2.[22] When probe wavelength is longer than 620 nm, $\Delta A_2(\lambda)$ is positive and induced absorption is the dominant process.

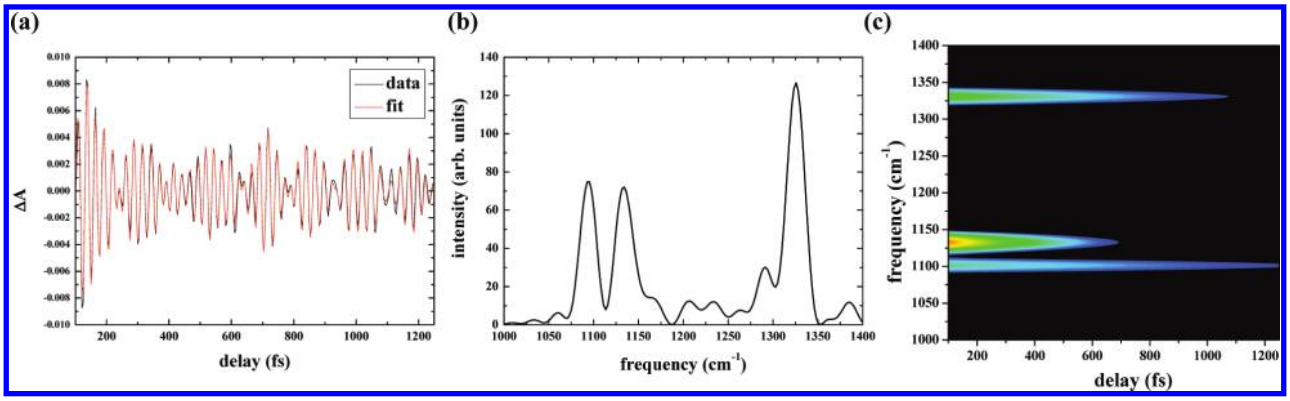

Figure 4. (a) Time trace of DR19 in solution measured at 626 nm (black curves) and the time trace reconstructed in LP-SVD analysis (red curves). (b) Fourier power spectrum of the measured time trace shown in (a). (c) Two dimensional view of the intensity of the vibrational modes obtained in the LP-SVD analysis.

Table 1. Results Obtained in the LP-SVD Analysis for DR19 in Solution

frequency (cm^{-1})	amplitude	decay (fs)
1100	107	2510
1131	285	458
1330	141	1411

The time constant τ_3 was determined to be 5.86 ± 2.13 ps. Its spectral component, $\Delta A_3(\lambda)$, has a flat profile with a positive value reflecting induced absorption. Koller et al.[10] elucidated that vibrational cooling in the ground state occurs in 4-nitro-40-(dimethylamino)azobenzene with a time constant of 5.5 ps. Therefore, τ_3 is assigned to the vibrational cooling time in the ground state of DR19.

Next, we have analyzed the oscillation observed in the time traces shown in Figure 2c,d. The periodic oscillations reflect molecular vibrations that occur during the reaction after photoexcitation; these oscillations have been theoretically studied[23] and observed in various experiments.[19,24,25] Fourier transform of the time trace measured at 626 nm (see Figure 4a) was calculated as shown in Figure 4b. It agrees with Raman spectrum,[26] confirming that the oscillations in the time-resolved trace are caused by molecular vibrations.

The vibrational dynamics was analyzed using linear prediction and singular value decomposition (LP-SVD).[27−29] Table 1 shows the frequencies, amplitudes, and lifetimes of the vibrational modes obtained in the LP-SVD analysis. The obtained parameters are also shown as a two-dimensional view in Figure 4c. When the obtained parameters were used, the time trace was reconstructed, as shown in Figure 4a, agreeing with the measured time trace. The vibration modes of 1100, 1131, and 1330 cm^{-1} are assigned to Φ−N stretching, C−H deformation, and NO_2 symmetric stretching modes, respectively, referring to the Raman study.[26] The result of the LP-SVD analysis shows that the C−H deformation has distinctly high amplitude and fast lifetime among these three vibration modes. It reflects that photoisomerization of the DR19 in solution causes large deformation around the C−H bond in its primary process.

Comparison with Ultrafast Dynamics of the Film Sample. Figure 5a shows a two-dimensional plot of the Δ*A* spectrum of the DR19 film sample measured for delays from −0.1 to 1.4 ps (short delay region) and probe wavelengths from 514 to 758 nm. Figure 5b shows the Δ*A* spectrum measured between −1 and 14 ps (long delay region) in the same probe wavelength region. The black curves in Figure 5a,b are contours for which Δ*A* is zero. Figure 5c,d show Δ*A* traces at five different probe wavelengths in Figure 5a,b.

Similar to the solution sample, the negative Δ*A* at delays shorter than 580 nm is assigned to absorption bleaching caused by depletion of the ground state and the positive Δ*A* observed at probe wavelengths longer than 580 nm reflects induced absorption of the excited state.

The Δ*A* traces of the film sample in Figure 5c,d also include three decay components with lifetimes of ∼0.1, ∼1, and ∼10 ps. Therefore, the Δ*A* traces were fitted in the same manner as the traces of the solution sample.

We first fitted the Δ*A* trace in the long delay region using eq 2 for delays from 0.4 to 14 ps. Global fitting analysis estimated the time constants of τ_2 and τ_3 to be 1.35 ± 0.19 and 5.77 ± 0.81 ps, respectively. The spectral components of the obtained time constants were obtained by the least-squares method (see Figure 6).

Compared with this data for DR19 in the film sample, ΔA_2 has a large positive amplitude in the wavelength region reflecting existence of induced absorption longer than 620 nm in solution (see Figure 3). The reason why the induced absorption appears in the solution sample of DR19 is thought to be explained as follows. The DR19 has a push−pull substituted structure with a large dipole moment of 8 D, and the solvent of TMTE is a polar solvent with a dipole moment of 3 D. Therefore, there is a strong dipole interaction between the DR19 and the solvent in the solution sample. The strong interaction modifies the electronic states of the higher excited state, which opens a way for the induced absorption via transition from the first excited state to the higher excited state.

The shortest time constant (τ_1) and its spectral component (ΔA_1) were then estimated by fitting the Δ*A* trace in the short delay region from 50 fs to 1.4 ps. Global fitting of the Δ*A* traces using eq 3 estimated the time constant τ_1 to be 74 ± 10 fs. The spectral component of τ_1 ($\Delta A_1(\lambda)$) was obtained by the least-squares method and is plotted in Figure 6.

The shortest time constant, τ_1, was estimated to be 74 ± 10 fs. For the same reason, given above for the solution sample, the shortest decay component was attributed to a large amplitude wave packet motion on the excited-state potential surface out of the FC region. The negative spectrum of ΔA_1 was considered to

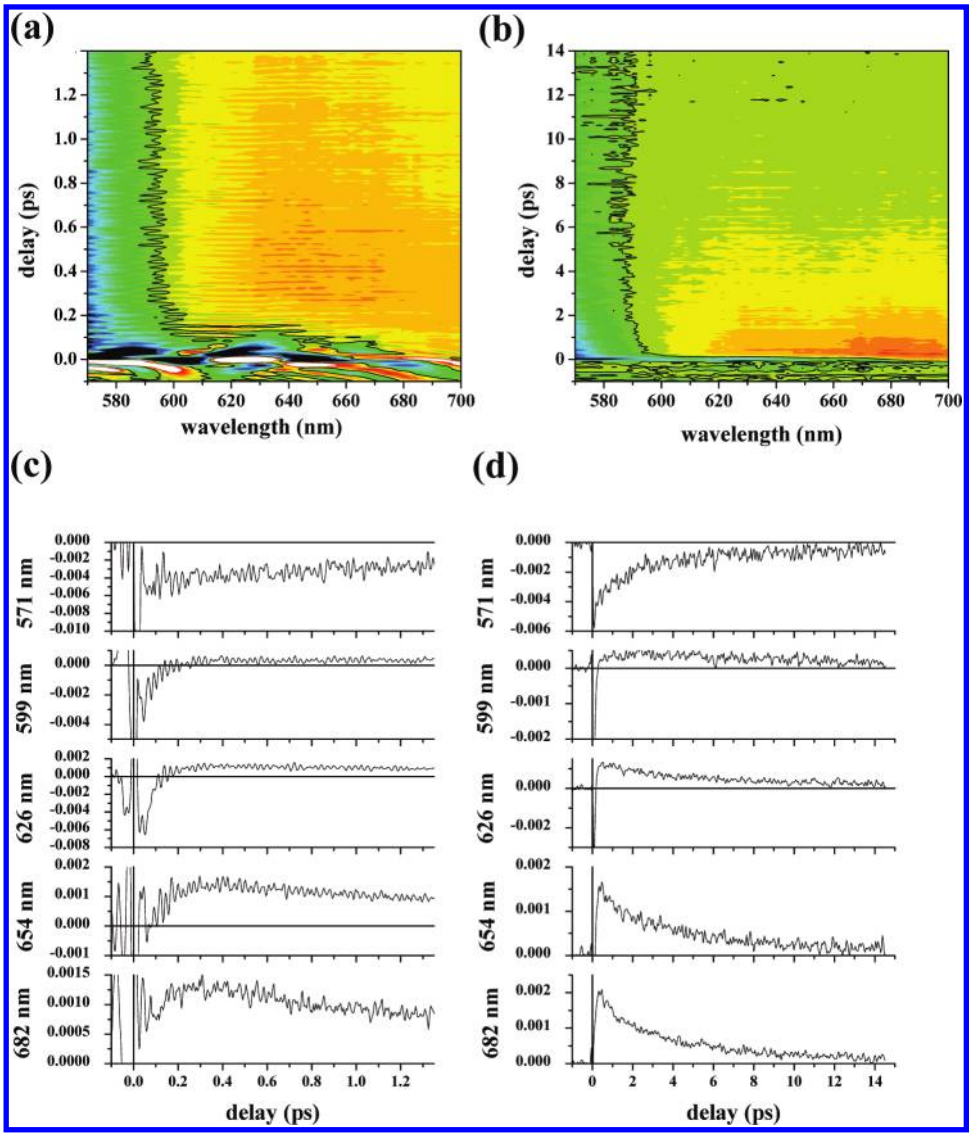

Figure 5. Measured 2D time-resolved absorbance difference spectra of DR19 in a film sample (a) scanned from −0.1 to 1.4 ps and (b) that scanned from −1 to 14 ps. Black curves represent contours where the absorbance change is zero ($\Delta A = 0$). (c, d) Time-resolved ΔA traces at five typical probe wavelengths picked up from (a) and (b), respectively.

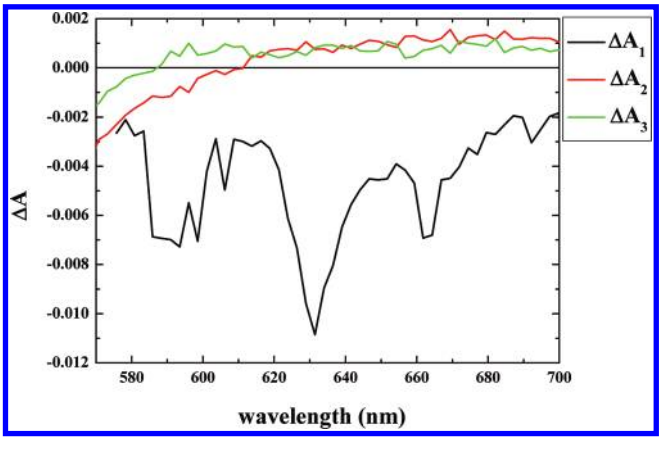

Figure 6. ΔA_1, ΔA_2, and ΔA_3 are spectral components of the DR19 film sample, which decay with the lifetimes of τ_1, τ_2, and τ_2, respectively.

be the stimulated emission spectrum of the FC state. DR19 is known to have a large dipole moment of up to 8 D[12,13] because of its push−pull substituted structure. Therefore, photoexcitation of DR19 generates a charge-transfer (CT) state via electron transfer. Inter- and intramolecular modes adapt within τ_1 to the new charge distribution generated by CT excitation. The solution and film samples had similar shortest time constant τ_1, which implies that solutions and films of DR19 have comparable adaptation speeds.

The time constant τ_2 is estimated to be 1.35 ± 0.19 ps. $\Delta A_2(\lambda)$ is negative at wavelength below 610 nm reflecting the spectral profile of the stationary absorption spectrum. Therefore, τ_2 in the film sample was also assigned to the time for the photoexcited wave packet in the excited state to find the conical intersection to the ground state via photoisomerization around the NN double bond; this process is responsible for the time constant τ_2. When probe wavelength is longer than 610 nm, $\Delta A_2(\lambda)$ is positive and induced absorption is the dominated process.

dx.doi.org/10.1021/jp2051307 |J. Phys. Chem. A 2011, 115, 11508–11514

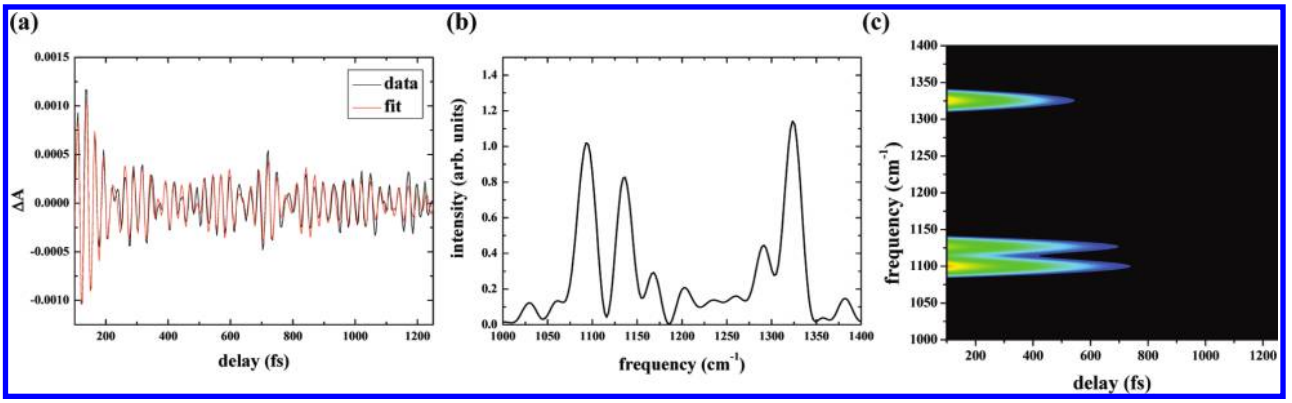

Figure 7. (a) Time trace of DR19 in a film sample measured at 626 nm (black curves) and the time trace reconstructed in LP-SVD analysis (red curves). (b) Fourier power spectrum of the measured time trace shown in (a). (c) Two dimensional view of the intensity of the vibrational modes obtained in the LP-SVD analysis.

Table 2. Results Obtained in the LP-SVD Analysis for DR19 in a Film Sample

frequency (cm^{-1})	amplitude	decay (fs)
1099	35	518
1126	27	588
1324	36	369

The time constant of τ_3 was determined to be 5.77 ± 0.81 ps. Its spectral component, $\Delta A_3(\lambda)$, has a flat profile with a positive induced absorption. Just as for the solution sample, τ_3 reflects the vibrational cooling time in the ground electronic state of DR19.

Fourier transform of the time trace measured at 626 nm (see Figure 7a) was also calculated for DR19 in a film sample as shown in Figure 7b. It agrees with the result obtained for solution sample (see Figure 4b) and Raman spectrum.[26] The LP-SVD analysis was performed for the time trace of the film sample. Table 2 shows the frequencies, amplitudes, and lifetimes of the vibrational modes obtained in the LP-SVD analysis. The obtained parameters are also shown as a two-dimensional view in Figure 7c. When the obtained parameters were used, the time trace was reconstructed as shown in Figure 7a, agreeing with the measured time trace. The assignments of 1099, 1126, and 1324 cm^{-1} are the same as those of the solution sample assigned to Φ−N stretching, C−H deformation, and NO_2 symmetric stretching modes, respectively, referring the Raman study.[26] The result of the LP-SVD analysis shows that all of those three modes have similar amplitude and fast lifetime of ∼500 fs. It reflects that photoisomerization of the DR19 in the film sample causes structural deformation equally among Φ−N bond, C−H bond, and NO_2 group. The result is significantly different from that of the DR19 in solution, which only the C−H deformation was dominantly excited. It is thought to be that the strong dipole interaction between TMTE and DR19 in the solution sample suppresses deformations along the dipole moment of the DR19 only allowing the C−H deformation.

SUMMARY

The photoisomerization of DR19 in solution and a polymer film were investigated absorbance difference measurements over a broadband visible spectral range and with a time resolution of 9 fs. The DR19 has a push−pull substituted structure, which forms the CT state via electron transfer after photoexcitation. Therefore, the film sample may have different dynamics from the solution sample because significant intermolecular CT in the film modifies the relaxation pathway of the CT state. The observed time traces contain three decay components with lifetimes of ∼0.1, ∼1, and ∼10 ps. We estimated the three time constants (τ_1, τ_2, and τ_3) and their spectral components (ΔA_1, ΔA_2, and ΔA_3) by fitting the time-resolved ΔA trace with a triple exponential function.

The shortest time constant, τ_1, had been roughly estimated in previous studies. In this study, τ_1 was precisely estimated for both the solution sample (104 ± 12 fs) and film (74 ± 10 fs) samples. Its spectral component, ΔA_1, is negative, reflecting stimulated emission from the FC state. The τ_1 decay component was attributed to a large amplitude wave packet motion on the excited-state potential surface out of the FC region.

The spectral component, $\Delta A_2(\lambda)$, is negative reflecting the spectral profile of the stationary absorption spectrum for probe wavelengths shorter than 580 nm. This implies that the wave packet generated by the photoexcitation is spread over the potential energy surface of the electronic excited state and finds the conical intersection to the ground state via photoisomerization around the NN double bond; this process is responsible for the time constant of τ_2.

The longest spectral component, $\Delta A_3(\lambda)$, has a flat profile and is positive due to induced absorption. Its time constant, τ_3, is much longer than τ_2, reflecting the vibrational cooling time in the ground electronic state of DR19.

In the present study, we clarified the ultrafast dynamics of a push−pull substituted azobenzene dye, DR19, which is known to have a large dipole moment and is promising for various applications. Ultrafast time-resolved absorbance difference spectroscopy is expected to provide essential information for photonic applications and is a promising alternative method for evaluating switching performance.

AUTHOR INFORMATION

Corresponding Author

*E-mail: yabushita@mail.nctu.edu.tw; cwluo@mail.nctu.edu.tw.

ACKNOWLEDGMENT

This work was supported by the National Science Council of Taiwan, ROC, under Grant Nos. NSC95-2112-M-009-011-MY3,

NSC96-2923-M-009-001-MY3, and NSC98-2112-M-009-008-MY3 and by the Grant MOE ATU Program at NCTU.

REFERENCES

(1) Kumar, G. S.; Neckers, D. C. *Chem. Rev.* **1989**, *89*, 1915–1925.
(2) Rau, H.; Lüddecke, E. *J. Am. Chem. Soc.* **1982**, *104*, 1616–1620.
(3) Stuart, C. M.; Frontiera, R. R.; Mathies, R. A. *J. Phys. Chem. A* **2007**, *111*, 12072–12080.
(4) Curtis, R. D.; Hilborn, J. W.; Wu, G.; Lumsden, M. D.; Wasylishen, R. E.; Pincock, J. A. *J. Phys. Chem.* **1993**, *97*, 1856–1861.
(5) Natansohn, A.; Rochon, P.; Gosselin, J.; Xie, S. *Macromolecules* **1992**, *25*, 2268–2273.
(6) Bian, S.; Kuzyk, M. G. *Opt. Lett.* **2002**, *27*, 1761–1763.
(7) Zhang, W.; Bian, S.; Kim, S.; Kuzyk, M. G. *Opt. Lett.* **2002**, *27*, 1105–1107.
(8) Jung, C. C.; Rutloh, M.; Stumpe, J. *J. Phys. Chem. B* **2005**, *109*, 7865–7871.
(9) Muraoka, T.; Kinbara, K.; Aida, T. *Nature* **2006**, *440*, 512–515.
(10) Koller, F. O.; Sobotta, C.; Schrader, T. E.; Cordes, T.; Schreier, W. J.; Sieg, A.; Gilch, P. *Chem. Phys.* **2007**, *341*, 258–266.
(11) Poprawa-Smoluch, M.; Baggerman, J.; Zhang, H.; Maas, H. P. A.; De Cola, L.; Brouwer, A. M. *J. Phys. Chem. A* **2006**, *110*, 11926–11937.
(12) Park, B.; Paoprasert, P.; In, I.; Zwickey, J.; Colavita, P. E.; Hamers, R. J.; Gopalan, P.; Evans, P. G. *Adv. Mater.* **2007**, *19*, 4353–4357.
(13) Choi, J. M.; Lee, J.; Hwang, D. K.; Kim, J. H.; Im, S.; Kim, E. *Appl. Phys. Lett.* **2006**, *88*, 043508.
(14) Mistler, R. E. *Am. Ceram. Soc. Bull.* **1998**, *77*, 82–86.
(15) Dürr, H.; Bouas-Laurent, H. *Photochromism: Molecules and Systems*; Elsevier: Amsterdam; Boston, 2003; pp 165−192.
(16) Shirakawa, A.; Sakane, I.; Kobayashi, T. *Opt. Lett.* **1998**, *23*, 1292–1294.
(17) Shirakawa, A.; Sakane, I.; Takasaka, M.; Kobayashi, T. *Appl. Phys. Lett.* **1999**, *74*, 2268–2270.
(18) Kobayashi, T.; Baltuska, A. *Meas. Sci. Technol.* **2002**, *13*, 1671–1682.
(19) Yabushita, A.; Lee, Y. H.; Kobayashi, T. *Rev. Sci. Instrum.* **2010**, *81*, 063110.
(20) Barrett, C. J.; Natansohn, A. L.; Rochon, P. L. *J. Phys. Chem.* **1996**, *100*, 8836–8842.
(21) Schmidt, B.; Sobotta, C.; Malkmus, S.; Laimgruber, S.; Braun, M.; Zinth, W.; Gilch, P. *J. Phys. Chem. A* **2004**, *108*, 4399–4404.
(22) Chang, C. W.; Lu, Y. C.; Wang, T. T.; Diau, E. *J. Am. Chem. Soc.* **2004**, *126*, 10109–10118.
(23) Pollard, W. T.; Lee, S.-Y.; Mathies, A. *J. Chem. Phys.* **1990**, *92*, 4012–4029.
(24) Polli, D.; Lüer, L.; Cerullo, G. *Rev. Sci. Instrum.* **2007**, *78*, 103108.
(25) Yabushita, A.; Kobayashi, T. *J. Phys. Chem. B* **2010**, *114*, 4632–4636.
(26) Marino, I. G.; Bersami, D.; Lottici, P. P.; Tosini, L.; Montero, A. *J. Raman Spectrosc.* **2000**, *31*, 555–558.
(27) Barhuijsen, H.; De Beer, R.; Bovee, W. M. M. J.; Creyhgton, J. H. N.; Van Ormondt, D. *Magn. Reson. Med.* **1985**, *2*, 86–89.
(28) Barhuijsen, H.; De Beer, R.; Van Ormondt, D. *J. Magn. Reson.* **1985**, *64*, 343–346.
(29) Johnson, A. E.; Myers, A. B. *J. Chem. Phys.* **1996**, *104*, 2497–2507.